Production of neutron-rich isotopes from the fragmentation of ^{28}Si projectiles at $p_{lab} = 14.6$ GeV/c per nucleon

J. Barrette,[3] R. Bellwied,[6,a] P. Braun-Munzinger,[6] W.E. Cleland,[5] G. David,[6,b] J. Dee,[6] O. Dietzsch,[7] E. Duek,[1,c] M. Fatyga,[1] D. Fox,[2,d] S.V. Greene,[9,e] J.R. Hall,[4,a] T.K. Hemmick,[9,f] N. Herrmann,[6,g] B. Hong,[6] K. Jayananda,[5,h] D. Kraus,[5] B. Shiva Kumar,[9] R. Lacasse,[3] D. Lissauer,[1] W.J. Llope,[6,i] T. Ludlam,[1] S.K. Mark,[3] S. McCorkle,[1] J.T. Mitchell,[9,j] M. Muthuswamy,[6,k] E. O'Brien,[1] C. Pruneau,[3,a] F.S. Rotondo,[9] N.C. da Silva,[7] J. Simon-Gillo,[8,l] U. Sonnadara,[5] J. Stachel,[6] E.M. Takagui,[5,m] H. Takai,[1] T.G. Throwe,[1] L. Waters,[6,l] C. Winter,[9] K. Wolf,[8] D. Wolfe,[4] C.L. Woody,[1] N. Xu,[6,l] Y. Zhang,[6] Z. Zhang,[5] and C. Zou[6]

(E814 Collaboration)

[1] *Brookhaven National Laboratory, Upton, New York 11973*
[2] *Los Alamos National Laboratory, Los Alamos, New Mexico 87545*
[3] *McGill University, Montreal, Canada*
[4] *University of New Mexico, Albuquerque, New Mexico 87131*
[5] *University of Pittsburgh, Pittsburgh, Pennsylvania 15260*
[6] *State University of New York, Stony Brook, New York 11794*
[7] *Universidade de São Paulo, São Paulo, Brazil*
[8] *Texas A&M University, College Station, Texas 77843*
[9] *Yale University, New Haven, Connecticut 06511*

(Received 1 November 1994)

An investigation of the production of neutron-rich isotopes from the fragmentation of ^{28}Si projectiles at p_{lab}=14.6 GeV/c per nucleon was performed using the BNL-AGS-E814 spectrometer. We have measured the inclusive production cross sections of neutron-rich fragments (^{6}He, ^{8}He, ^{8}Li, ^{9}Li, ^{10}Be, ^{11}Be, and ^{13}B). We have also measured the transverse momentum distributions for ^{6}He and ^{9}Li, and the forward and transverse energy distributions associated with ^{6}He production. The momentum distributions were analyzed in the context of the Goldhaber model. The question of whether the fragments are produced in the decay of the projectile following its electromagnetic excitation was also investigated.

PACS number(s): 25.75.+r

I. INTRODUCTION

Data from fragmentation studies have been a valuable source of information used to better understand the composition of cosmic rays [1], to aid the search for exotic nuclei and, recently, to study the production of secondary exotic nuclear beams [2]. In the past few years, heavy ion beams with ultrarelativistic energies have become available at the CERN-SPS and BNL-AGS accelerators. These facilities provide a unique opportunity to investigate projectile fragmentation in an energy regime where data is rather scarce. Ideas and concepts developed to understand data from measurements at lower energies, mainly at the Bevalac, can now be tested in a new energy domain.

The fragmentation of relativistic heavy ions can be induced by either nuclear or electromagnetic interaction. For nuclear interactions, the cross sections are dominated by the geometry of the collision [3]. In the limiting frag-

[a]Present address: Dept. of Physics, Wayne State University, Detroit, MI 48202.
[b]Present address: Brookhaven National Laboratory, Building 510A, Upton, NY 11973.
[c]Present address: SSC Laboratory, MS 1070, 2550 Beckleymeade Ave., Dallas, TX 75248.
[d]Present address: Chalk River Nuclear Labs, Chalk River, ON, Canada K07 1J0.
[e]Present address: Dept. of Physics, Vanderbilt University, Nashville, TN 37235.
[f]Present address: Dept. of Physics, State University of New York, Stony Brook, NY 11794.
[g]Present address: Physikalisches Institut, Universität Heidelberg, D 69 Heidelberg, Germany.
[h]Present address: Dept. of Physics, University of Sri Jayewardenepura, Nugegoda, Sri Lanka.
[i]Present address: Dept. of Physics, Michigan State University, East Lansing, MI 48824.
[j]Present address: Nuclear Science Division, Lawrence Berkeley Laboratory, Berkeley, CA 94720.
[k]Present address: Dept. of Radiation Oncology, Presbyterian Hospital, Pittsburgh, PA 15260.
[l]Present address: Los Alamos National Laboratory, Los Alamos, NM 87545.
[m]Present address: Universidade de São Paulo, São Paulo, SP 05508, Brazil.

mentation hypothesis [4] the production cross sections have no energy dependence for projectile energies above a few GeV per nucleon. The level of agreement between predictions of semiempirical relations [1, 5] and experimental data at or beyond AGS energies has yet to be established. The momentum distributions can be described by the Goldhaber model [6]. In this model, the fragment momentum is the vector sum of the momentum of its nucleons before the collision, which is related to the Fermi momentum of the parent nucleus. This interpretation assumes no momentum transfer to the fragment. However, studies [7] have shown fragment momentum distributions that are wider than expected, indicating the possible presence of secondary processes in the collision. There is also evidence [8] that the momentum distributions change with the centrality of the collision.

For electromagnetic interactions the measured cross sections and the final state energy distributions [9, 10] for particle emission can be explained by the excitation of the giant dipole resonance (GDR) through the absorption of virtual photons from the target field and subsequent nuclear deexcitation [11, 12]. The cross sections depend strongly on the target atomic number and on the bombarding energy [11], as the number of virtual photons rapidly increases with both. The high density of virtual photons suggests that the double GDR could be excited by the absorption of two photons. Estimates of the cross sections for the electromagnetic excitation of the double GDR of a ^{28}Si projectile on a Pb target at AGS energies range from 7 mb to 20 mb [11–13]. It has also been suggested [12–14] that the large collective oscillations of protons against neutrons in the double GDR could lead to the breakup of nuclei into fragments rich in protons or neutrons. Experimental evidence on the excitation of the double GDR has been recently reported [15–18].

In this paper we investigate the production of neutron-rich fragments ($Z/A \leq 0.4$) in collisions of ^{28}Si projectiles at $p_{\rm lab} = 14.6$ GeV/c per nucleon with Al, Cu, Sn, and Pb targets. Since fragmentation with complete isotope identification has not been previously studied at AGS energies, the determination of fragmentation production cross sections and momentum distributions can provide new valuable information on the production mechanism. We also investigate the possibility of producing these fragments through the decay of the electromagnetically excited projectile.

II. EXPERIMENTAL SETUP

The E814 experimental setup has been extensively described in other publications [9, 10]. A schematic view of the apparatus is given in Fig. 1. It allows multiplicity measurements and it has a 4π calorimetric coverage around the target, for event characterization. A high resolution forward spectrometer detects the particles emitted in an angular range of ± 18.4 (horizontal) and ± 12.3 (vertical) mrad relative to the beam direction.

The detectors around the target are *target calorimeter* (TCal), consisting of 992 NaI crystals assembled in four side walls surrounding the target and one back wall (see Ref. [19] for further details); *target scintillators* (TPad), made up of 52 plastic scintillator slats lining the inside walls of the TCal; *participant calorimeter* (PCal), a Pb/scintillator segmented calorimeter (see Refs. [20, 21] for construction and calibration details); *silicon multiplicity detectors* (Mult), two silicon disks of 512 pads each (see Ref. [22] for further details).

The forward spectrometer consists of one cathode pad readout chamber (DC1) [23] located between the two dipole magnets (M1 and M2) and two hybrid pad and drift chambers (DC2 and DC3) [24, 25] positioned downstream of the second magnet; *magnet scintillators* (MSci), 16 plastic scintillator slats lining the inside walls of the two magnets; *forward scintillators* (FSci), two hodoscopes, one (10 counters) positioned 12 m and the other (39 counters) 31 m downstream from the target; and forward *uranium calorimeters* (UCal), 25 U/Cu/scintillator segmented modules (see Ref. [26] for details), positioned downstream of the FSci.

The beam is defined by a set of scintillators (BSci) placed upstream of the target. Two silicon strip detectors (BVer) are used as tracking devices, defining the horizontal position and angle of incidence of beam particles at the target on an event by event basis. To make a precise identification of the charge of the projectile and tag an interaction in the target, the pulse height is measured in two silicon detectors 1 cm in diameter and 100 μm thick placed just upstream and downstream of the target.

The forward spectrometer (see Refs. [9, 10, 27] for further details) is extensively used in the present analysis [28]. The identification of the fragment charge is accomplished by the forward scintillators, which are plastic scintillators of dimensions $10\times1\times120$ cm^3, read out at both ends by photomultiplier tubes. The charge measurement (proportional to the geometrical average of the pulse heights recorded at each end) has a resolution of 3% and allows the unambiguous identification of particles with atomic number Z=1 to Z=14. The energy of the particles is measured by the UCal [26]. The UCal modules are segmented in 12 optically decoupled sections, each read out by two wavelength shifter bars coupled to photomultiplier tubes. The segmentation of the calorimeter permits the location of the center of the shower to within 2 cm. The calorimeters indicated by the hatched area in Fig. 1 are used in the trigger system to select neutron-rich fragments with beam rapidity and $0.2 \leq Z/A \leq 0.4$, where A is the fragment mass number.

The tracking devices, from which the momentum vectors are obtained, are the three chambers, DC1, DC2 and DC3, discussed in Refs. [23–25]. DC2 and DC3 are similar except for the size and number of wires. They were designed to be sensitive to a wide range of charge deposition, with 300 μm single cell position resolution from minimum ionizing to Z=14 particles.

The large gaps in the forward spectrometer are filled with helium bags to reduce the amount of material along the fragment path. This procedure decreases the number of interactions downstream of the analyzing magnets. Nevertheless a 30% loss of beam particles (^{28}Si) has been measured in the 36 m flight path after the target. Targets of natural Al (1.30 g/cm^2), Cu (2.24 g/cm^2), Sn

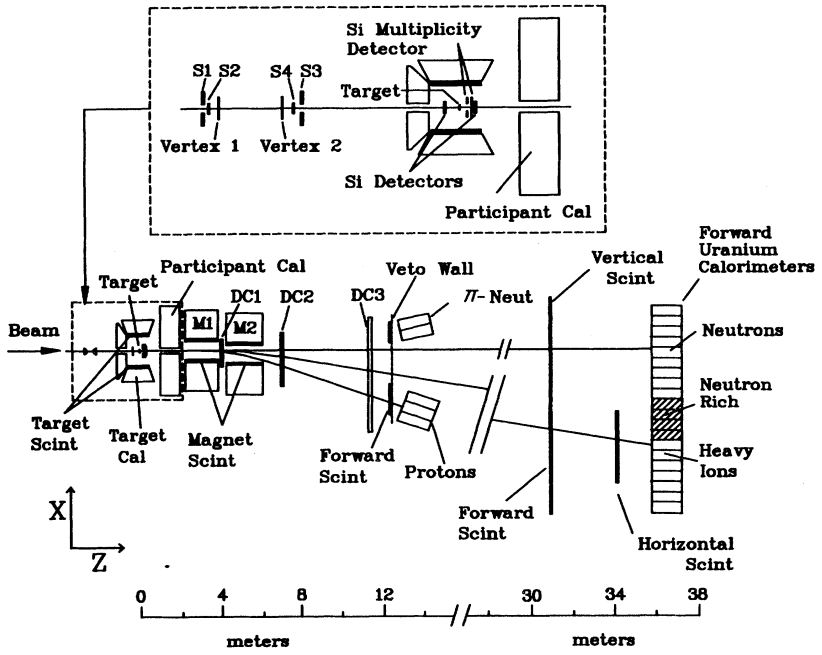

FIG. 1. The E814 experimental setup. The incident beam passes through a hole in the target calorimeter back wall. Forward emitted particles pass through the participant calorimeter opening and through magnets M1 and M2. Track positions are measured in chambers DC1, DC2, and DC3. Charge is measured by energy loss in the forward scintillators and energy is measured in the forward uranium calorimeters. The hatched area shows the calorimeter elements used in the trigger logic.

(3.35 g/cm^2), and Pb (4.36 g/cm^2), all with a thickness of ~4% of a ^{28}Si nuclear interaction length, were used. Data were also taken with an empty target holder in order to evaluate interactions not originating in the target.

The E814 trigger system is designed to allow data taking with parallel triggers, with the possibility of reducing (*downscaling*) a fraction of the higher rate triggers, thus enhancing the fraction of rare events in a given data sample. The *neutron-rich trigger* was set to select events where neutron-rich isotopes ($0.2 \leq Z/A \leq 0.4$) with beam rapidity were produced. This trigger is implemented in two levels. The first level requires the presence of a beam particle and energy deposition greater than 7.5 GeV in the calorimeters labeled "neutron-rich" (hatched in Fig. 1). At the second level it is required that more than 60 GeV of energy be deposited in this same region. In addition, a reaction in the target is required, as indicated by the pulse height measured in the downstream silicon detector. The upper charge limit for accepting an event was set to the peak position corresponding to a $Z=13$ particle. This requirement is made in order to minimize triggering on interactions occurring downstream of the target. Once a trigger occurs, digitized information from all detectors is written to magnetic tape. There are no significant trigger biases other than the minimum energy requirement in the neutron-rich region imposed by the second level trigger. The data sample corresponds to an integrated number of beam particles of $\sim 3 \times 10^7$ for each target. Since these data were collected in parallel with other triggers, only one in six neutron-rich triggers was written to tape. Integral luminosities range from 0.17 μb^{-1} for the Al target to 0.056 μb^{-1} for the Pb target.

III. DATA REDUCTION AND ANALYSIS

The data analysis is made in two steps. In a first stage cuts are applied in order to reject spurious events. Beam particles are selected by requiring that the energy loss of the particle in the beam scintillators and in the upstream silicon detector be within specified limits. The resolution for this energy loss measurement is approximately 5%. Criteria based on the FSci and UCal information are used to select events with $Z \geq 2$. With all cuts in place, information from the selected events is used as input to the tracking analysis procedure.

The tracking procedure consists of the following steps [10].

(1) A cluster search is performed in the active area of DC1 and in the pad and drift sections of DC2 and DC3 where neutron-rich isotopes with beam rapidity are expected.

(2) Pad clusters from DC1, DC2, and DC3 are combined with wire hits from DC2 and DC3, UCal clusters, the FSci hit pattern and the silicon vertex detector hits and input to the track reconstruction program.

(3) Track fitting is performed, using the fragment rigidity as a variable in the fit. The trajectory of the beam particle before the target and the reconstructed downstream trajectory are required to match at the target. Due to the lack of measurements of the vertical position before the target, the vertical position of the vertex is assumed to be at the origin, within the vertical dispersion of the beam (± 1 mm).

Isotope identification is made based on the three following parameters assigned to each particle: (i) momentum vectors from the tracking procedure, (ii) charge, as measured by the energy loss in the forward scintillators, and (iii) energy, as measured in the forward uranium calorimeter. Figure 2 shows a plot of energy loss in the forward scintillators (charge) vs magnetic rigidity for reconstructed events. The isotope separation is further improved by requiring a match between the fragment momentum and the energy deposited in the calorimeter. For

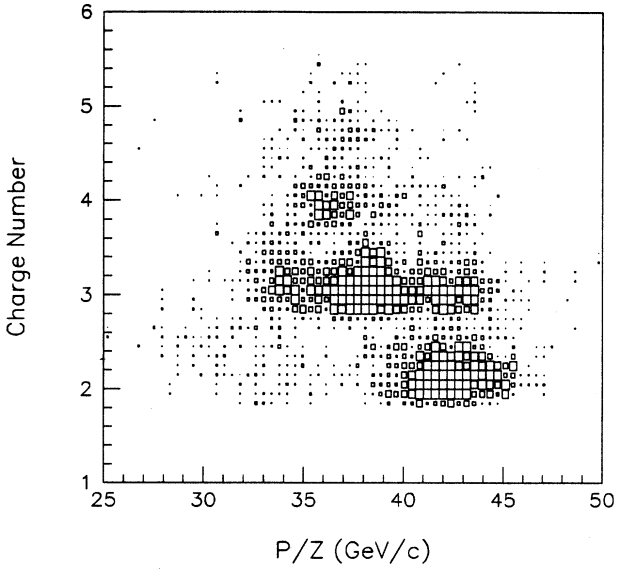

FIG. 2. Area plot of energy loss (charge) of fragments, as measured in the forward scintillators vs magnetic rigidity (P/Z) measured in the downstream spectrometer. Isotopes of beam rapidity are cleanly identified in such a plot [37]. The overlap between isotopes is due to the spread in momentum rather than tracking resolution. Isotope identification is improved by the use of energy information from the forward calorimeters. In the histogram, the maximum number of counts per bin was limited to 10 to provide a better view of the low statistics regions.

each event containing a neutron-rich fragment two other global quantities were used for event characterization: the zero degree energy E_0 (the energy in the forward uranium calorimeters) and the transverse energy E_T (measured in the participant and target calorimeters). The production cross sections were determined for ^{6}He, ^{8}He, ^{8}Li, ^{9}Li, ^{10}Be, ^{11}Be, and ^{13}B. Due to statistics limitations, momentum distributions were determined only for ^{6}He and ^{9}Li.

The measured cross sections are corrected for the acceptance of the apparatus with the aid of a Monte Carlo simulation. For this simulation, we assume a momentum distribution for the fragment of the form [6]

$$f(p_i) \propto \exp(-p_i^2/2\sigma^2), \quad i = x, y, z, \tag{1}$$

with

$$\sigma^2 = \sigma_0^2 K(A-K)/(A-1), \tag{2}$$

where K is the mass number of the fragment, A the mass number of the parent nucleus, and σ_0 is a parameter to be adjusted. The fragments are then transported through the spectrometer, and spatial coordinates are generated in all tracking devices and at the face of the forward calorimeters, allowing a direct comparison between simulated and experimental events. The energy loss of the beam particle and of the fragment in the target as well as in other parts of the experiment is included in the simulation. The energy deposit in the UCal is also simulated [26].

The correction factors for the cross sections due to geometrical acceptance depend on the value of the width σ of the momentum distributions. For ^{6}He and ^{9}Li, the value of σ is obtained from the measured momentum distributions (which are discussed in Sec. IV). For the other fragments we used the values of σ obtained from Eq. (2) with a value of σ_0 extracted from the measured ^{6}He and ^{9}Li momentum distributions. In estimating the errors in the correction factors for the fragments for which we did not have the full momentum distributions, we assume an error on the value of σ_0 of $(^{+20}_{-10})\%$. This error is based on an analysis of the applicability of Eq. (2) to the set of fragmentation data of Greiner *et al.* [29] for ^{16}O and ^{12}C projectiles at 2 GeV/c per nucleon.

The simulation allows the correction of measured quantities due to geometrical acceptance and trigger biases. A fraction of the events is not detected because fragments of interest with low momentum hit the forward calorimeters outside the neutron-rich trigger region shown in Fig. 1. All cross sections are corrected for the geometrical acceptance, which ranges from 98% to 50% for all isotopes except ^{13}B and ^{10}Be, whose acceptance values are 17% and 6%, respectively.

The second level trigger threshold on the UCal energy (60 GeV) introduces a bias for ^{6}He. The fluctuation in energy deposition causes some events to yield a measured energy below the threshold. Furthermore, some fragments hit the calorimeter at the edge of the trigger region and the shower may not be entirely contained within it. The losses were evaluated including both the energy fluctuation and shower profile in the simulation [26]. Approximately 5% of ^{6}He are lost due to these effects.

Rather than simulating the loss of fragments due to secondary interactions, either in the target or between the target and the trigger calorimeters, we have simply estimated the probability for the process using the geometrical cross sections of the fragments, combined with a detailed accounting for all materials downstream of the target. Losses in the fragment yield due to these downstream interactions range from (13±2)% for ^{6}He to (20±2)% for ^{13}B.

The total systematic uncertainty for ^{6}He production cross sections is of the order of ±15%, most of it due to the trigger bias. For ^{8}He and ^{9}Li, the systematic uncertainties are small (<5%). For the other fragments the systematic uncertainties are mostly due to the corrections for geometrical acceptance: ±10% for ^{8}Li and ^{11}Be, $(^{+50}_{-30})\%$ for ^{13}B, and $(^{+90}_{-50})\%$ for ^{10}Be. The systematic uncertainties in the widths of the measured momentum distributions (^{6}He and ^{9}Li), due to uncertainties in the beam momentum, field strength, and effective length of the spectrometer magnets, as well as position resolution of the tracking devices, are about 3%.

IV. RESULTS AND DISCUSSION

The cross sections for the production of neutron-rich isotopes are presented in Table I. As shown in Fig. 3,

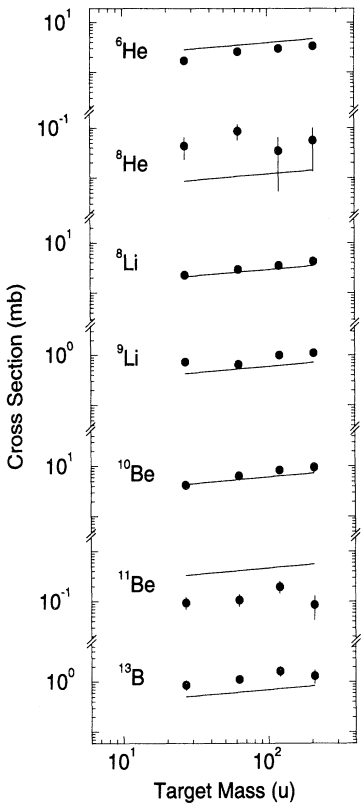

FIG. 3. Cross sections for the production of ^{6}He, ^{8}He, ^{8}Li, ^{9}Li, ^{10}Be, ^{11}Be, and ^{13}B, obtained from ^{28}Si on Al, Cu, Sn, and Pb at $p_{\rm lab}$ = 14.6 GeV/c per nucleon. The solid curves are extrapolations from lower energy data using the semiempirical formulation of Silberberg and Tsao [33]. Error bars represent statistical uncertainties only.

they exhibit a slow increase as a function of the target mass. This increase is well described by a functional dependence of the form

$$\sigma \propto A_P^{1/3} + A_T^{1/3}, \tag{3}$$

which implies that the majority of the fragments are produced in peripheral nuclear collisions.

Information on the geometry of the collision is obtained from the forward energy (E_0) and transverse energy (E_T) distributions for the events. For beam rapidity fragments (projectile spectators) the forward energy is a direct measure of the number of projectile nucleons that did not participate in collisions with the target. In Fig. 4, E_0 distributions for three targets (Al, Cu, and Pb) are shown for events where a ^{6}He ion is detected.

The minimum energy seen in the forward calorimeters is consistent with the ^{6}He ion remaining as the only projectile spectator. Using a simple geometric model [30], we estimate that the maximum overlap between target and projectile is approximately 5 fm for all targets. The maximum forward energy corresponds to a very peripheral nuclear collision, with almost all of the projectile energy being detected in the forward calorimeters. The average number of nucleons that remain as projectile spectators is 19 for the Al target and 17 for the Pb target. According to the geometrical model, this corresponds to an overlap of approximately 2 to 3 fm for these targets. These numbers should be compared to the radii of the projectile (3.6 fm) and of the targets (3.6 fm for Al and 7.1 fm for Pb) used in the calculations.

The PCal ($0.9 < \eta < 3.9$) transverse energy distributions for events in which a ^{6}He ion is produced in interactions with the Al, Cu, and Pb targets are shown in Fig. 5. No leakage corrections are needed due to the low values of E_T for these events [21]. The transverse and the forward energy are correlated variables and the corresponding distributions are consistent with each other. The distributions have maxima around 10 GeV for Al and 15 GeV for the Pb target, with few events producing E_T values of 30 GeV or more. Inspection of data in Ref. [31] shows that for very central Si+Al collisions the produced E_T can reach values of the order of 60 GeV.

It would be interesting to compare the absolute magnitude of the cross sections to similar data obtained at Bevelac energies (1–2 GeV per nucleon). Unfortunately, no such data are available for ^{28}Si. However, cross sections can be estimated using the semiempirical formulation of Silberberg and Tsao [1, 32], in which the limiting fragmentation hypothesis is assumed to hold above ~2 GeV per nucleon. A set of parameters for this formulation was obtained by Crawford *et al.* [33] from fits to

TABLE I. Cross sections for the production of neutron-rich isotopes from ^{28}Si projectiles at $p_{\rm lab}$ = 14.6 GeV/c per nucleon interacting with Al, Cu, Sn, and Pb targets. The errors shown are statistical uncertainties only. The cross sections scale uncertainties (systematic errors) are <5% for ^{8}He and ^{9}Li, ±10% for ^{8}Li and ^{11}Be, ±15% for ^{6}He, $(^{+50}_{-30})$% for ^{13}B, and $(^{+90}_{-50})$% for ^{10}Be.

Fragment	σ(Al) (mb)	σ(Cu) (mb)	σ(Sn) (mb)	σ(Pb) (mb)
^{6}He	1.70 ± 0.13	2.60 ± 0.16	3.00 ± 0.23	3.40 ± 0.29
^{8}He	0.04 ± 0.02	0.09 ± 0.03	0.03 ± 0.03	0.06 ± 0.04
^{8}Li	2.29 ± 0.19	2.93 ± 0.24	3.51 ± 0.34	4.30 ± 0.46
^{9}Li	0.73 ± 0.08	0.65 ± 0.08	1.01 ± 0.13	1.11 ± 0.17
^{10}Be	4.21 ± 0.74	6.39 ± 0.97	8.3 ± 1.4	9.5 ± 1.9
^{11}Be	0.09 ± 0.03	0.11 ± 0.03	0.20 ± 0.05	0.09 ± 0.04
^{13}B	0.87 ± 0.18	1.12 ± 0.22	1.64 ± 0.35	1.32 ± 0.40

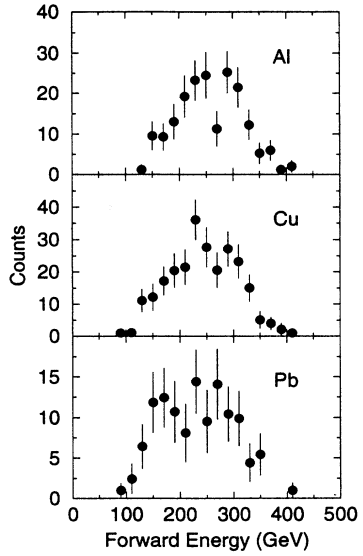

FIG. 4. Forward energy distribution, E_0, associated with the production of ^{6}He fragments, as measured in the forward calorimeter (UCal). The error bars are statistical uncertainties.

a data base for heavy ion fragmentation cross sections. The expected production cross sections so obtained for the neutron-rich isotopes investigated in the present work are shown in Fig. 3 (solid lines) together with our measured values.

There is overall agreement between the present data and the extrapolated values for the cross sections. The discrepancy for ^{11}Be and ^{8}He may reflect the lack of data for neutron-rich isotopes in the database. The parameters of Ref. [33], used in the present work, are adjusted for secondaries commonly found in the cosmic ray data, such as the proton-rich nucleus ^{7}Be. Inclusion of the present data in the database could contribute to improve the cross section estimates for such isotopes.

For the production of ^{11}Li and ^{12}Be, the estimated cross sections for the Pb target are 3 μb and 20 μb, respectively. A search for these rarer isotopes was carried out. Two events were found for which ^{11}Li was identified, one each for the Cu and Pb targets. The corresponding production cross sections are 7 μb and 18 μb, respectively. No ^{12}Be events were found.

Distributions for the three components of the momentum vector were obtained from the tracking procedure. Due to the low statistics available, results are presented only for ^{6}He and ^{9}Li fragments. Within statistics, the distributions for the different targets are similar and thus were added for the extraction of the momentum width parameters. Distributions for the two transverse components p_x and p_y were evaluated (p_y is the direction perpendicular to the bending plane). Figure 6 shows the distributions for these components for ^{6}He and ^{9}Li. Also shown are Gaussian fits to the data. The corresponding parameters of the fits to the transverse momentum distributions are presented in Table II.

The contribution of multiple scattering and energy loss in both the target and the materials between the target and the tracking devices is found to be negligible. The

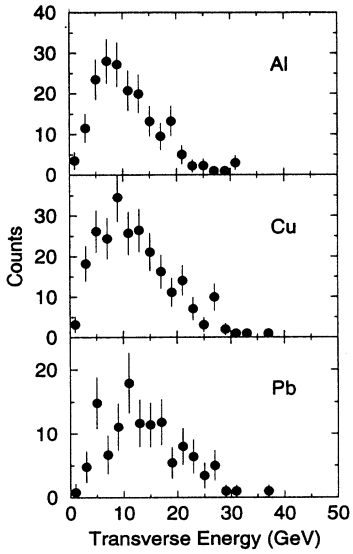

FIG. 5. Transverse energy distribution, E_T, associated with the production of ^{6}He fragments, as measured in the participant calorimeter (PCal). The error bars are statistical uncertainties.

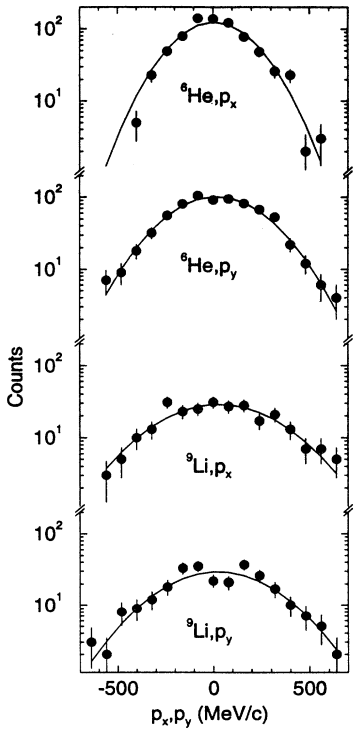

FIG. 6. Momentum distributions, p_x and p_y (p_y perpendicular to the magnet bending plane), for ^{6}He and ^{9}Li fragments. The solid curves are Gaussian fits to the data. The error bars are statistical uncertainties.

TABLE II. Adjusted values for the width of the p_x and p_y (p_y perpendicular to the magnet bending plane) distributions and deduced values for σ_0 and p_F.

Fragment	$\sigma(p_x)$ (MeV/c)	$\sigma(p_y)$[a] (MeV/c)	σ_0[b] (MeV/c)	p_F[b] (MeV/c)
^{6}He	188±20	226±12	94±5	210±11
^{9}Li	281±12	278±27	111±6	248±13

[a]Corrected for experimental resolution.
[b]Calculated from the average values of p_x and p_y.

position resolution in the horizontal direction causes no significant broadening of the horizontal momentum distribution. However, the position resolution in the vertical direction, of ~0.2 cm for DC2 and ~0.3 cm for DC3, contributes to the broadening of the momentum distribution in this direction and was subtracted quadratically from the adjusted values in order to obtain the quantities shown in Table II. As discussed in Sec. III, the ^{6}He data are affected by acceptance inefficiencies in the low momentum region. Therefore, only the data for $p_x \geq 0$ were used in fitting the Gaussian (centered at 0 MeV/c).

In Goldhaber's [6] interpretation of the fragmentation process, the fragment is formed combining K nucleons, which are randomly chosen from a nucleus with A nucleons and net momentum $\vec{p}_A = 0$. In this model, the width of the momentum distribution of the produced fragments is given by Eq. (2), and σ_0 is related to the Fermi momentum of the parent nucleus by $p_F = \sigma_0\sqrt{5}$, as previously suggested by Feshbach and Huang [34]. The values obtained from the present data for σ_0 are 94±5 MeV/c and 111 ± 6 MeV/c for ^{6}He and ^{9}Li, respectively. These values correspond to a Fermi momentum for ^{28}Si of 210±11 MeV/c and 248±13 MeV/c from the ^{6}He and ^{9}Li data, respectively. The Fermi momentum for ^{24}Mg obtained from electron scattering experiments is 235±5 MeV/c [35]. Fragmentation data for ^{12}C and ^{16}O projectiles exist for beam energies around 1–2 GeV per nucleon [29], from which was obtained a Fermi momentum of 178±5 MeV/c for ^{12}C and 185±3 MeV/c for ^{16}O.

Data presented in Ref. [36] suggest that the width of the fragment momentum distribution increases with increasing centrality of the collision. Subsequently, it was found [8] that for light fragments (p, d, α) the width of the momentum distributions indeed depends on centrality. For fragments such as ^{4}He or ^{6}He an increase in the width should be observed only for very high centrality events where the present data have poor statistics.

We have also investigated the possibility that neutron-rich isotopes are produced electromagnetically. The energy-integrated total cross section for the excitation of the ^{28}Si double GDR calculated in Ref. [12] is 20 mb. Events with production of fragments via electromagnetic dissociation should not produce signals in the detectors surrounding the target; also, due to the low transverse momentum produced in this type of reaction, our forward spectrometer has full acceptance for the fragments, implying that all the projectile energy should be seen in the forward calorimeters. We have made use of these characteristics for the measurement of the cross sections for the removal of a few nucleons via EMD [9, 10, 37]. For this analysis, as in Refs. [9, 10, 37], we require (i) very low multiplicity in the target scintillator pads, at the level of the δ-electron background; (ii) energy deposition in the TCal below 20 MeV; (iii) low multiplicity in the silicon multiplicity detector, also at the level of the δ-electron background; and (iv) total energy deposition of less than 1 GeV (with less than 200 MeV per cell) in the PCal.

The entire data sample contains only one event with a ^{6}He fragment that meets the above requirements, observed in an interaction with a Pb target. Also, both the downstream silicon detector signal and the parameters of the fit of the trajectory by the tracking algorithm indicate that the fragment originates in the target. The energy deposited in the forward calorimeters is equal, within the resolution of the detector, to the total energy carried by the beam particle.

The ^{6}He EMD event candidate includes three to four protons and no neutrons, with the remaining fragments in the beam region ($Z/A \simeq 0.5$). Even considering a final state with the lowest threshold (^{6}He+3p+^{19}F), the Q value would be −59.5 MeV and it seems therefore unlikely that such an event would originate from ^{28}Si electromagnetic dissociation in the Pb target field. It is also known from a previous analysis [10] that very peripheral nuclear reactions may have similar signatures as those for EMD reactions. Although the background due to nuclear reactions can be subtracted statistically from the EMD data through the cross section dependence on the target Z [10], it is impossible to carry it out on an event by event basis. Based on this data sample, we estimate for the Pb target an upper limit of 54 μb (at the confidence level of 95%) for the EMD cross section into any of the examined channels. We conclude that electromagnetic dissociation does not contribute significantly to the production of neutron-rich isotopes in projectile fragmentation.

To summarize, we have presented a measurement of cross sections for neutron-rich isotope production from a 14.6 GeV/c per nucleon ^{28}Si beam incident on several targets. Our results indicate that these fragments are produced in semiperipheral collisions with an average radial overlap between the target and projectile of approximately 2 to 3 fm. Within the precision of the measurements both the cross sections and the momentum width distributions are consistent with lower energy fragmentation studies. In the data sample collected, corresponding to approximately 3×10^7 integrated beam particles for each target, there are no events originating from EMD into neutron-rich isotopes.

ACKNOWLEDGMENTS

We acknowledge the excellent support by the BNL AGS and Tandem staffs and Dr. Y. Makdisi and Dr. H. Brown for expert help in design and running of our beam line. The help of H. J. Crawford in obtaining the extrapolated values for the cross sections from the database of fragmentation cross section measurements is gratefully acknowledged. This research is partially supported by the U.S. Department of Energy, the National Science Foundation, the National Science and Engineering Research Council of Canada and the Conselho Nacional de Desenvolvimento Científico e Tecnológico (CNPq-Brazil).

[1] R. Silberberg and C.H. Tsao, Phys. Rep. **191**, 351 (1990).
[2] I. Tanihata, in *Proceedings of The Rio de Janeiro Workshop on Relativistic Aspects of Nuclear Physics*, edited by T. Kodama, K.C. Chung, S.J.B. Duarte, and M.C. Nemes (World Scientific, Singapore, 1989), p. 157.
[3] D.L. Olson, B.L. Berman, D.E. Greiner, H.H. Heckman, P.J. Lindstrom, and H.J. Crawford, Phys. Rev. C **28**, 1602 (1983).
[4] J. Benecke, T.T. Chou, C.N. Yang, and E. Yen, Phys. Rev. **188**, 2159 (1969).
[5] J.R. Cummings, W.R. Binns, T.L. Garrard, M.H. Israel, J. Klarmann, E.C. Stone, and C.J. Waddington, Phys. Rev. C **42**, 2508 (1990).
[6] A.S. Goldhaber, Phys. Lett. **53B**, 306 (1974).
[7] F.P. Brady *et al.*, Phys. Rev. Lett. **60**, 1699 (1988).
[8] M. Muthuswamy *et al.*, E814 Collaboration, Nucl. Phys. **A544**, 423c (1992).
[9] J. Barrette *et al.*, E814 Collaboration, Phys. Rev. C **41**, 1512 (1990).
[10] J. Barrette *et al.*, E814 Collaboration, Phys. Rev. C **45**, 2427 (1992).
[11] C.A. Bertulani and G. Baur, Phys. Rep. **163**, 299 (1988).
[12] W.J. Llope and P. Braun-Munzinger, Phys. Rev. C **41**, 2644 (1990).
[13] P. Braun-Munzinger *et al.*, Proposal E814 submitted to the AGS Program Committee (1985).
[14] G. Baur and C.A. Bertulani, Phys. Lett. B **174**, 23 (1986).
[15] S. Mordechai *et al.*, Phys. Rev. Lett. **61**, 531 (1988).
[16] J. Ritman *et al.*, Phys. Rev. Lett. **70**, 533 (1993).
[17] R. Schmidt *et al.*, Phys. Rev. Lett. **70**, 1767 (1993).
[18] T. Aumann, J.V. Kratz, E. Stiel, K. Sümmerer, W. Brüchle, M. Schädel, G. Wirth, M. Fauerbach, and J.C. Hill, Phys. Rev. C **47**, 1728 (1993).
[19] J. Barrette *et al.*, E814 Collaboration, Phys. Rev. Lett. **64**, 1219 (1990); J. Barrette *et al.*, E814 Collaboration, Phys. Rev. C **45**, 819 (1992); L.S. Waters, Ph.D. thesis, SUNY-Stony Brook, 1991.
[20] J. Simon-Gillo *et al.*, Nucl. Instrum. Methods Phys. Res. Sect. A **309**, 427 (1991); D. Fox *et al.*, *ibid.* **317**, 474 (1992); Z. Zhang, Ph.D. thesis, University of Pittsburgh, 1993.
[21] Z. Zhang, P. Braun-Munzinger, W. Cleland, G. David, and D. Lissauer, Nucl. Instrum. Methods Phys. Res. Sect. A **343**, 610 (1994).
[22] J. Barrette *et al.*, E814 Collaboration, Phys. Rev. C **46**, 312 (1992); M.K. Jayananda, Ph.D. thesis, University of Pittsburgh, 1991.
[23] B. Yu, Ph.D. thesis, University of Pittsburgh, 1991.
[24] J. Fisher *et al.*, IEEE Trans. Nucl. Sci. **37**, 82 (1990).
[25] R. Debbe *et al.*, IEEE Trans. Nucl. Sci. **37**, 88 (1990).
[26] M. Fatyga, D. Makowiecki, and W.J. Llope, Nucl. Instrum. Methods Phys. Res. Sect. A **284**, 323 (1989).
[27] U. Sonnadara, Ph.D. thesis, University of Pittsburgh, 1992.
[28] N.C. da Silva, Ph.D. thesis, University of São Paulo, Brazil, 1994.
[29] D.E. Greiner, P.J. Lindstrom, H.H. Heckman, B. Cork, and F.S. Bieser, Phys. Rev. Lett. **35**, 152 (1975).
[30] J. Gosset, H.H. Gutbrod, W.G. Meyer, A.M. Poskaner, A. Sandoval, R. Stock, and G.D. Westfall, Phys. Rev. C **16**, 629 (1977).
[31] J. Barrette *et al.*, E814 Collaboration, Phys. Rev. Lett. **70**, 2996 (1993).
[32] R. Silberberg and C.H. Tsao, Astrophys. J. Suppl. Ser. 220 **25**, 315 (1973). See also G. Rudstam, Z. Phys. **21a**, 1027 (1966), for the original formulation.
[33] H.J. Crawford, J. Engelage, P. Ferrando, T.G. Guzik, F.C. Jones, P.J. Lindstrom, J.W. Mitchell, A. Soutoul, C.J. Waddington, W.R. Webber, and J.P. Wefel, "A database of fragmentation cross section measurements applicable to cosmic ray propagation calculations," LBL Report No. 27725, 1991.
[34] H. Feshbach and K. Huang, Phys. Lett. **47B**, 300 (1973).
[35] E.J. Moniz, I. Sick, R.R. Whitney, J.R. Ficenec, R.D. Kephart, and W.P. Trower, Phys. Rev. Lett. **26**, 445 (1971).
[36] M.I. Adamovich *et al.*, Phys. Rev. C **40**, 66 (1989).
[37] J. Barrette *et al.*, E814 Collaboration, Phys. Rev. C **51**, 865 (1995).